Ore Geology Reviews 65 (2015) 42–54

Contents lists available at ScienceDirect

Ore Geology Reviews

journal homepage: www.elsevier.com/locate/oregeorev

Structural control and genesis of the Oligocene Zhenyuan orogenic gold deposit, SW China

Jun Deng *, Qingfei Wang, Gongjian Li, Yan Zhao

State Key Laboratory of Geological Processes and Mineral Resources, China University of Geosciences, Beijing 100083, China

ARTICLE INFO

Article history:
Received 16 December 2012
Received in revised form 13 August 2014
Accepted 13 August 2014
Available online 20 August 2014

Keywords:
Zhenyuan
Continental underthrust
Orogenic gold deposit
Ailaoshan

ABSTRACT

The Zhenyuan gold deposit with >50 t gold reserve is located within the Jinshajiang–Ailaoshan suture zone that formed through the closure of Paleo-Tethyan ocean in late-Permian. This suture separates the Simao and South China blocks. A west-dipping high velocity zone down to ca. 250 km beneath the Simao block in the seismic tomography suggests that the South China lithosphere was underthrust westward. The NNW-trending Ailaoshan–Red River shear zone is situated to the east of Ailaoshan suture. The shearing in this belt, generally following a regional mantle upwelling and crust extension event, was initiated at 32 Ma and culminated at ca. 27 Ma. This shearing was induced by the lateral extrusion and large clockwise rotation of the Simao block during the India–Eurasia continental collision and the underthrusting of South China block. The Zhenyuan ore deposit consists of the Donggualin and Laowangzhai orebody clusters. The Donggualin orebodies are controlled by the NW-striking shear faults, whereas most orebodies in the Laowangzhai are dominated by NE- and ENE-striking transcompressional faults. It is observed that the NE- and ENE-striking faults are crosscut by the NW-striking faults. It is deduced that the former were primarily formed as nearly NS-trending faults during the regional extension or initial shearing stage at ca. 32 Ma. The primary faults were then re-oriented to the current strike concomitant with the rotation of the Simao block, and further cut by the NW-trending shear faults, which are subsidiary to the Ailaoshan–Red River shear zone. The rock types in the ore deposit including slate, meta-sandstone, limestone, lamprophyre, and meta-mafic to ultramafic units, which were all mineralized by the infiltration of ore-bearing fluids into extensional fractures. The low temperature ore mineral assemblage (pyrite–stibnite–arsenopyrite), enriched element association, and ranges of S and Pb isotopic compositions in the two ore clusters are broadly similar, indicating that the mineralization is contemporary despite the different formation times of ore-controlling structures. The $^{206}Pb/^{204}Pb$, $^{207}Pb/^{204}Pb$, and $^{208}Pb/^{204}Pb$ values of hydrothermal pyrite are close to those of the lower crust. Pyrite $\delta^{34}S$ values show a wide range with a peak near 0 per mil. The S and Pb isotopic compositions, together with previously published H–O–He–Ar isotopic data, suggest that the ore fluid is mainly metamorphic. The data also suggest the input of mantle volatiles, consistent with mantle upwelling. The control of the shear zones on mineralization favors the interpretation that the Ar–Ar isochron age ~27 Ma of phlogopite in the mineralized lamprophyre represents the mineralization age. This mineralization age implies that the South China block had started westward underthrusting before ~27 Ma. The Zhenyuan ore deposit is considered to be an orogenic type, formed in a transitional stage from mantle upwelling to continental underthrust. The continental underthrusting drove the release of gold-charged metamorphic fluids and formation of the Zhenyuan ore deposit.

1. Introduction

The Ailaoshan tectonic belt is an important tectonic–magmatic–metallogenic belt in the Sanjiang region, SW China. This belt comprises the Ailaoshan–Red River shear zone (ASRRSZ) in the east and the Ailaoshan suture in the west (Lai et al., 2014a,b; Wang et al., 2014; Zaw et al., 2014). The Ailaoshan suture was formed by the closure of one arm of the Paleo-Tethyan ocean in late-Permian (Deng et al., 2014a; Li et al., 2013b). The evolution of the belt in the Cenozoic was largely constrained by the India–Eurasia continental collision (Deng et al., 2010a,b, 2011; Hou and Cook, 2009; Lee and Lawver, 1995). It was proposed that the Ailaoshan belt experienced mantle upwelling and crust extension at ~35 Ma and followed by the intensive compressional shearing along the ASRRSZ (Leloup et al., 1995; Liu et al., 2012; Lu et al., 2012; Wang et al., 2001b). Along the belt, several hydrothermal gold deposits controlled by subsidiary shear zones, e.g. the Zhenyuan and Daping, occur to the west of the ASRRSZ (Hu et al., 1998; Yang et al., 2011). The Zhenyuan ore deposit containing more than 50 t Au is the largest shear zone-controlled gold deposit in the Sanjiang region.

* Corresponding author. Tel./fax: +86 10 82322301.
E-mail address: djun@cugb.edu.cn (J. Deng).

http://dx.doi.org/10.1016/j.oregeorev.2014.08.002
0169-1368/

The geological setting (Bi et al., 1996), auriferous fluids (Burnard et al., 1999; Liang et al., 2011; Zhao et al., 2013a), and metallogenic time (Wang et al., 2001a) of the ore deposit have been previously studied. However the detailed ore-controlling structures, genetic type and tectonic background remain ambiguous. In this paper, these issues are further taken up in combination with the previously published isotopic data.

2. Geological settings

2.1. Regional geology

SW China comprises several major tectonic blocks, i.e., the Sibumasu, Eastern Qiangtang, Western Qiangtang, Simao (the northern part of Indochina block), and South China blocks (Fig. 1). These blocks were amalgamated due to the closures of Tethyan oceans. The Jinshajiang suture developed in the northern Sanjiang and Ailaoshan suture in the southern Sanjiang were formed by closures of Paleo-Tethys oceanic arms in late-Permian (Deng et al., 2014a). In Cenozoic, the India–Eurasia continental collision caused the lateral extrusion of the Indochina block and the formation of several shear zones (Socquet and Pubellier, 2005).

The ASRRSZ is bordered by the east-dipping Ailaoshan and Red River faults, and it stretches over 100 km in length and about 1 to 3 km wide, striking N20–30°W and dipping N60–80°E (Hou et al., 2007) (Fig. 2). Between the Red River fault and the Ailaoshan fault is the Proterozoic Ailaoshan Group, which consists of high-grade metamorphic rocks (Burnard et al., 1999; Xiong et al., 2007) (Fig. 2). The left-lateral shearing along the ASRRSZ initiated at 31 Ma and culminated at ~27 Ma according to the zircon U–Pb ages of leucogranite dikes (Cao et al., 2011).

A belt with low-grade metamorphic rocks is developed west of the Ailaoshan fault. This unit comprises the Paleozoic rocks with metamorphic degrees from schist to slate, Ailaoshan suture, intrusive rocks with different emplacement ages, and numerous Cenozoic porphyry and shear zone-controlled ore deposits (Yang et al., 2011) (Fig. 2). The Ailaoshan suture separates the Simao block from the South China block (Fig. 1) (Wang et al., 2000). The Ailaoshan suture, formed by the closure of the Ailaoshan branch of Paleo-Tethyan ocean in late-

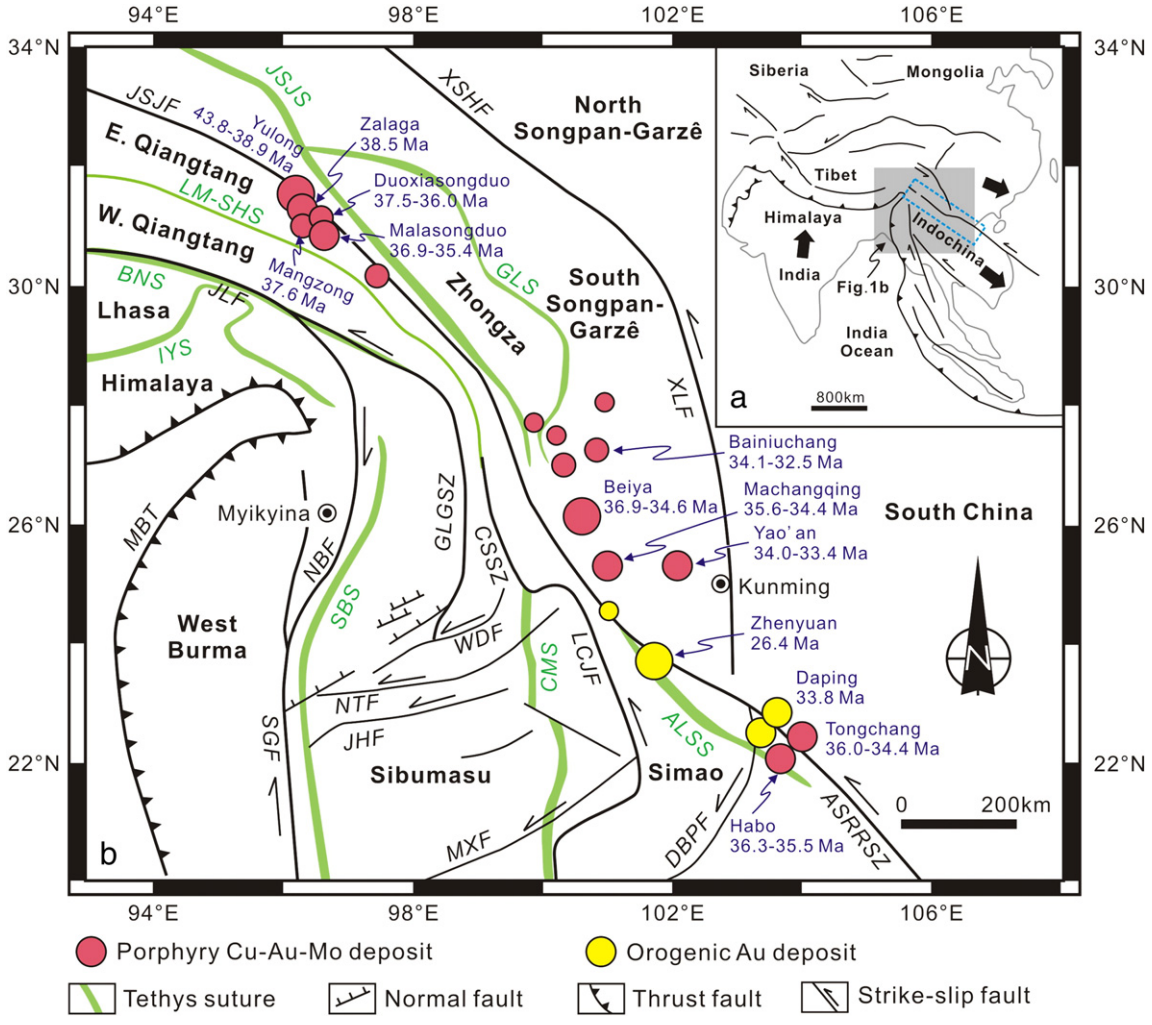

Fig. 1. (a) Simplified geological map showing major tectonic structures due to the collision between the India and Eurasia continents; (b) tectonic map of the SW China showing major tectonic units, Cenozoic faults and porphyry Cu–Au–Mo and orogenic Au deposit. Typical porphyry Cu–Au–Mo deposits constrained by zircon U–Pb and molybdenite Re–Os dating methods include: (1) Yulong, Zalaga, Mangzong, Duoxiasongduo, and Malasongduo in the northern Jinshajiang–Ailaoshan belt (Guo et al., 2006; Hou et al., 2006; Jiang et al., 2006; Liang et al., 2006, 2008; Tang et al., 2009; Wang et al., 2009), (2) Beiya, Machangqing, Yao' an, and Bainiuchang in the middle (He et al., 2013; Hou et al., 2006; Lu et al., 2012), and (3) Habo and Tongchang in the southern belt (Liang et al., 2007; Wang et al., 2005; Zhu et al., 2009). The orogenic Au deposit includes Zhenyuan (Wang et al., 2001a; phlogopite Ar–Ar inverse isochron age from a mineralized lamprophyre) and Daping (Sun et al., 2009; sericite Ar–Ar plateau age from sericitized diorite). Abbreviation: (1) Sutures: GLS, Garzê–Litang suture; JSJS, Jinshajiang suture; ALSS, Ailaoshan suture; LM–SHS, Longmucuo–Shuanghu suture; CMS, Changning–Menglian suture; BNS, Bangonghu–Nujiang suture; IYS, India river–Yalu-Zangbo suture; SBS, Shan Boundary suture; (2) major Cenozoic fault/shear zone: XSHF, Xianshuihe fault; XJF, Xiaojiang fault; ASRRSZ, Ailaoshan–Red River shear zone; LCJF, Lancangjiang fault; JLF, Jiali fault; CSSZ, Congshan shear zone; GLGSZ, Gaoligong shear zone; SGF, Sagaing fault; NBF, Nabang fault; MBT, Main boundary thrust fault; WDF, Wanding fault; NTF, Nanting fault; JHF, Jinghong fault; MXF, Mengxing fault; DBPF, Dien bien phu fault.
Modified after Socquet and Pubellier (2005), Metcalfe (2011), Xu et al. (2011) and Zi et al. (2012).

Permian, is represented by the Ailaoshan ophiolitic belt (Zhong, 1998). The ophiolitic belt comprises peridotites, gabbros, diabase, plagiogranite, and basalts (Mo et al., 1993). An array of subsidiary shear zones was developed in this unit (Leloup et al., 1995). The east-dipping Jiujia–Mojiang shear zone borders the lower-grade metamorphic unit on the west (Fig. 2).

Potassic mafic and felsic magmatic suites with ages of 42–32 Ma are exposed along the Jinshajiang–Ailaoshan suture (Guo et al., 2005; Sun et al., 2009; Zhang et al., 2010) (Fig. 1). The removal of the lower lithospheric mantle was suggested to have triggered the potassic magmatism (Lu et al., 2013). The potassic magmatism caused the formation of dozens of porphyry and skarn Cu (–Mo–Au) ore deposits, e.g., Yulong in the north, Beiya in the middle, and Habo in the south. In the Ailaoshan low-grade metamorphic unit, besides these porphyry ore deposits, several hydrothermal gold ore deposits controlled by the subsidiary shear zones are developed, including Zhenyuan in the northern part and Daping in the southern part. Seismic tomography reveals a west-dipping high velocity anomaly down to ca. 250 km beneath the Simao block (Liu et al., 2000). This high velocity anomaly is explained to represent a part of the plate of South China block underthrust in Cenozoic (Deng et al., 2014b; Flower et al., 2013).

In the background of India–Eurasia continental collision, several other shear zones, such as, Chongshan and Gaoligong shear zones, were formed in the Sanjiang region (Fig. 1) (Chung et al., 1997; Deng et al., 2014b; Leloup et al., 1995; Otofuji et al., 2011; Searle et al., 2010; Socquet and Pubellier, 2005; Yin and Harrison, 2000). Gold mineralization was barely developed along these shear zones compared to the ASRRSZ.

2.2. Deposit geology

The Zhenyuan ore deposit is mainly composed of Laowangzhai and Donggualin orebody clusters and several other segments with small gold reserves, such as Daqiaoqing, Kudumu, and Lannitang (Fig. 3). The Laowangzhai and Donggualin orebody clusters contain gold reserves of 18 t and 45 t respectively, (BGMRYP, 1993a,b). The Laowangzhai cluster is hosted by Carboniferous Suoshan Formation, which includes the argillaceous marble, slate (siliceous slate and sericite slate), and is hosted by extensively weathered diabase, basalt and ultramafic rocks of Permian age. The Donggualing cluster comprises the Upper Devonian Kudumu Formation, which is composed of sericite slate, siliceous slate, meta-quartz sandstone, argillaceous limestone, and a small portion of Carboniferous Suoshan Formation. Cenozoic lamprophyre and Mesozoic granitic dikes are widespread in both clusters (Huang et al., 2002). (See Fig. 3.)

3. Deposit structures and mineralization occurrences

3.1. Deposit structures

Structural observations and joint measurement were carried out in the pits of Donggualin and Laowangzhai ore clusters. The structure system is mainly dominated by steep NW-striking shear faults in the Donggualin cluster (Figs. 3, 4, 5) and nearly latitudinal to NE striking faults in the Laowangzhai cluster (Figs. 6, 7). In the Donggualin pit, the fault planes are nearly parallel. In the Laowangzhai pit, two NE-trending thrust faults bound several NW and nearly EW fault planes (Fig. 6). In the Donggualin cluster, the NW-trending faults are developed upon previous folds with NW-trending axles (Figs. 4, 5). In the ore deposit, the different lithologies in the Upper Devonian Kudumu Formation and Carboniferous Suoshan Formation, as well as the Permian and Cenozoic igneous rocks form a kind of mélange, reflecting intense shearing (Fig. 6). For instance, in the Laowangzhai, slices of diabase and meta-ultramafic rocks (serpentine) and the meta-sedimentary rocks in the Carboniferous Suoshan Formation are juxtaposed (Fig. 7). It is also shown that, in the Donggualin cluster, lamprophyre, and felsic dikes are discontinuously developed along the NW-trending faults, denoting a re-shaping process by shearing (Fig. 4c); and in the Laowangzhai pit, the pod-shaped granite is obviously faulted (Fig. 5).

According to the intense shearing, most primary rock beds were overprinted by jointing. A statistical study of joint fabrics was carried out nearby the fault planes in the two clusters. In the Donggualin ore cluster, the NW to NNW-trending joints are dominant, but some NE to ENE-trending joints are still present. These NE–ENE-trending joints were crosscut and severely re-worked by the NW-trending ones and only a small portion preserved (Fig. 4c). In the Laowangzhai, both the ENE-trending joints and NW-trending ones are present. The co-existence and intersecting of the two different trending joints suggest that the NE–ENE-trending faults were developed before the NW-trending ones instead of a secondary structure to the latter.

3.2. Mineralization

The amount of gold in different lithologies is listed in Table 1 based on the exploration report (BGMRYP, 1993a,b). The host lithology varies from one orebody to another. For instance, the slate, meta-sandstone, meta-mafic to ultramafic igneous rocks, granite, and limestone (including calcareous slate) occupy 12, 45, 39, 1, and 3% of the ore tonnage in orebody III_2 respectively, and they take 38, 17, 42, 2, and 1% in orebody IV_1 in the Laowangzhai cluster. In the Donggualing, the lamprophyre, meta-sandstone, slate plus limestone, and granite separately contain 26, 15, 46, and 13% of ore tonnage in orebody SII_1, 40, 19, 30, and 11% in orebody SII_2. These spatial variations reveal that the control of lithology on the mineralization in the Donggualing and Laowangzhai clusters is barely visible at the ore deposit scale.

The orebodies were controlled by the faults as shown in the pits and drill sections (Figs. 4, 5, 6, 7). The orebodies have the shape of veins and lens, characterized by dilation and contraction, thinning and emerging in strike and dip orientation, as shown in the drillhole sections (Figs. 5 and 7). Orebodies have NW strikes in the Donggualin cluster (Fig. 6) whereas those in the Laowangzhai are mainly in latitudinal or NE strikes (Fig. 7) in accordance with the strikes of the dominant faults in the clusters. In Donggualin, some orebodies turn into NW orientation gradually

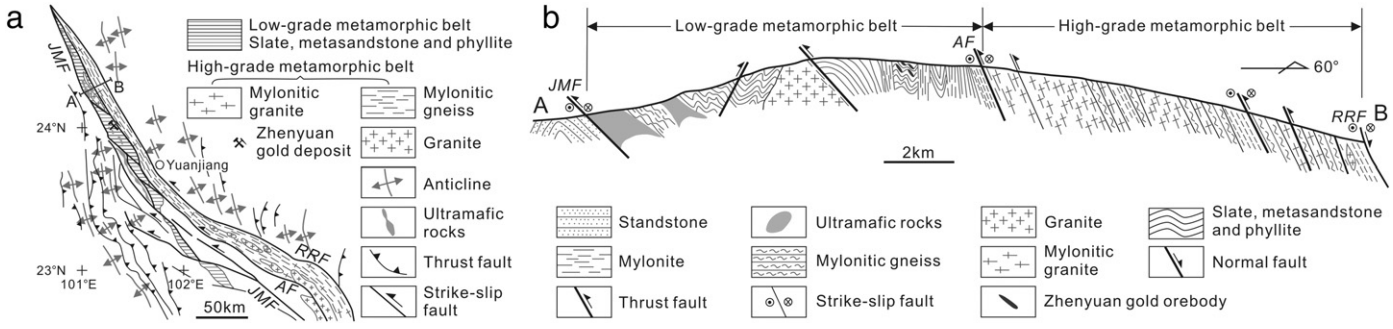

Fig. 2. Geological map (a) and cross-section (b) of the Ailaoshan tectonic belt, SW China. Abbreviation: AF, A' Mojiang fault; JMF, Jiujia–Mojiang fault; RRF, Red River fault. Revised from Hou et al. (2007) and Zhang et al. (2006).

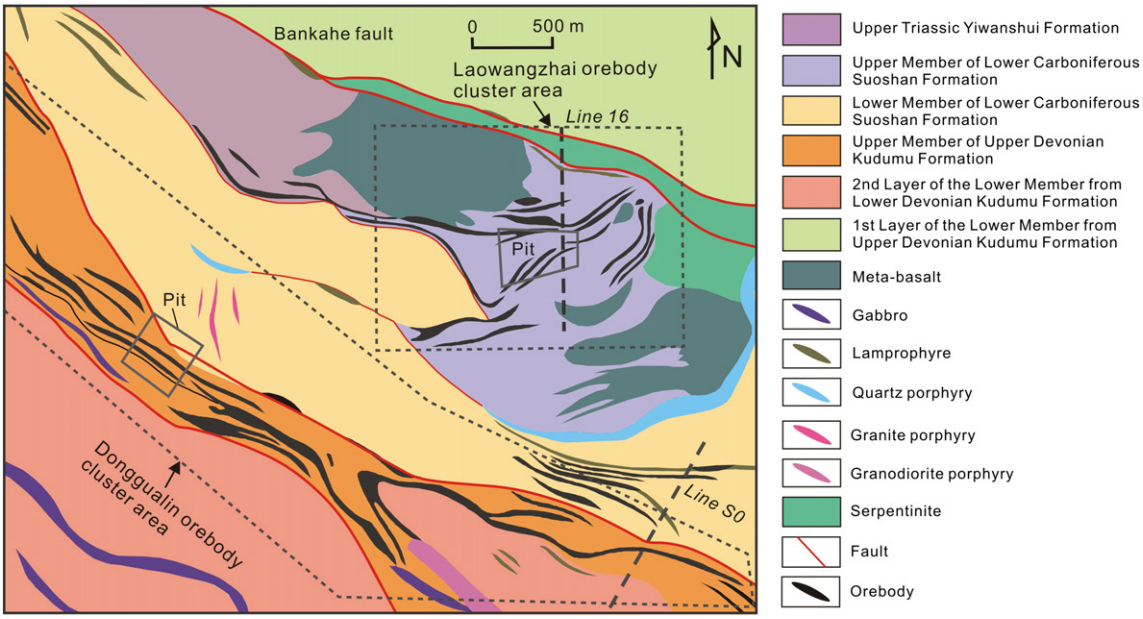

Fig. 3. Geological map of the Donggualin and Laowangzhai orebody clusters of the Zhenyuan ore deposit, SW China. Revised from BGMRYP (1993a).

as they extend to the Laowangzhai cluster (Fig. 3), suggesting that the NW-trending faults were connected with the previous NE or ENE-trending ones to channel the auriferous fluid. In the Donggualin drillhole section (Fig. 5), the steep faults connected several bed-parallel faults within the previous fold in the shallow part, and formed a complex orebody shape. In contrast, the orebody attitude in the Laowangzhai is relatively regular in the drill section. Sulfide veins and ore lenses occur in the extensional spaces in the fault zones (Fig. 4b, h).

Hydrothermal alteration of country rocks, including sericitization, pyritization, carbonatization, silicification, and chloritization, is significant. Ore minerals are pyrite, chalcopyrite, arsenopyrite, and stibnite. The ores have disseminated, meshlike (Fig. 8a), and brecciated structures (Fig. 8B). The meshlike structure suggests filling by the auriferous fluids into the brittle cracks (Fig. 8A), while the ore minerals experienced further fracturing in younger deformation as the brecciated textures denotes. Ore stages include quartz–pyrite, quartz–polymetallic sulfides, quartz–arsenopyrite–pyrite, and calcite–quartz–stibnite–pyrite (Zhao et al., 2013b). Gold occurs mainly as electrum or native gold contained in pyrite. Gangue minerals are quartz, ankerite, sericite, chlorite, and calcite.

4. Ore geochemistry

4.1. Analytical techniques

The samples from various lithologies and mineralization were collected systematically in the pits of the two clusters. For the whole-rock geochemical analyses, all samples were crushed into 200-mesh using an agate mill. The analyses were performed at the Geological Survey and Laboratory Center of Langfang, China. Major elements were determined by the standard X-ray fluorescence (XRF) method using a Philips Model 1480 spectrometer. Trace elements (As, B, Bi, Cd, Hg, Mo, Sb, W, Cu, Pb, Zn and Ag) were analyzed using inductively coupled plasma mass spectrometry (ICP-MS). The detection limits were ≤0.1 wt.% for major elements and ≤2 ppm for trace elements. Gold is determined by flameless atomic absorption spectroscopy (AAS) method with an uncertainty of 0.2 ppb.

Sulfur isotopic compositions of pyrites were analyzed using a MAT-252 isotope ratio mass spectrometer. Sulfide samples were combusted in the presence of excess CuO in vacuum to produce SO_2. The analytical precision is greater than 0.3‰, and the values are reported relative to the Canyon Diablo Troilite (CDT) (Li et al., 2013a).

Measurement of Pb isotopes was performed using a Nu Instrument multi-collector ICP-MS at the Laboratory of Isotope Geology, the Ministry of Land and Resources of China. A Tl-doping method similar to that described by Belshaw et al. (1998) was utilized. Repeat analyses of the NBS 981 Pb isotopic standard gave a reproducibility (2δ) of $^{208}Pb/^{206}Pb = 2.16736 \pm 0.00066$, $^{207}Pb/^{206}Pb = 0.91478 \pm 0.00028$, $^{206}Pb/^{204}Pb = 16.9386 \pm 0.0131$, $^{207}Pb/^{204}Pb = 15.4968 \pm 0.0107$, and $^{208}Pb/^{204}Pb = 36.7119 \pm 0.0331$ ($\pm 2\sigma$).

4.2. Analytical results

The samples analyzed in this study do not show any obvious preferential elemental enrichment with respect to the lithology (Supplementary Table; Fig. 9). The gold is contained in diverse lithologies, such as slates, granite and meta-sandstone, that are exposed in the pits. Slate is the most common host rock for mineralization. In the limestone, slate, meta-sandstone and granite, rocks with gold content greater than 0.1 g/t are more enriched in As, Ag and Sb than those with gold < 0.1 g/t. One lamprophyre sample with Au content around 10 g/t is remarkably enriched in As and Ag. Some samples with low Au content show high Sb concentration, which can be explained by a Sb-halo being formed around the Au orebody. This feature suggests that the gold-charged fluid generally has elevated content of As, Sb, and Ag.

The $\delta^{34}S$ values of the pyrite samples in the ore deposit vary widely, with most values lying between −4 to 2‰; and a peak at 0 per mil (Fig. 10, Table 2). The Laowangzhai orebody cluster shows $\delta^{34}S$ values similar to those in Donggualin (Fig. 10a), and the sulfides from different lithologies are also comparable. The $\delta^{34}S$ values of pyrite are not diagnostic of the ore sources, as the peak value is compatible with both mantle and average crustal reservoirs. The large variation of $\delta^{34}S$ can be explained by the mixing of the different sources or the oxidation effect of a reduced fluid (Hodkiewicz et al., 2009). Since oxidized phases are absent in the ores of this deposit, a mixing model is more favorable.

Lead isotopic compositions of auriferous pyrites in the Laowangzhai are 17.16–18.76, 15.38–15.74, and 37.47–39.24 for $^{206}Pb/^{204}Pb$, $^{207}Pb/^{204}Pb$, and $^{208}Pb/^{204}Pb$ respectively, and those in the Donggualin are

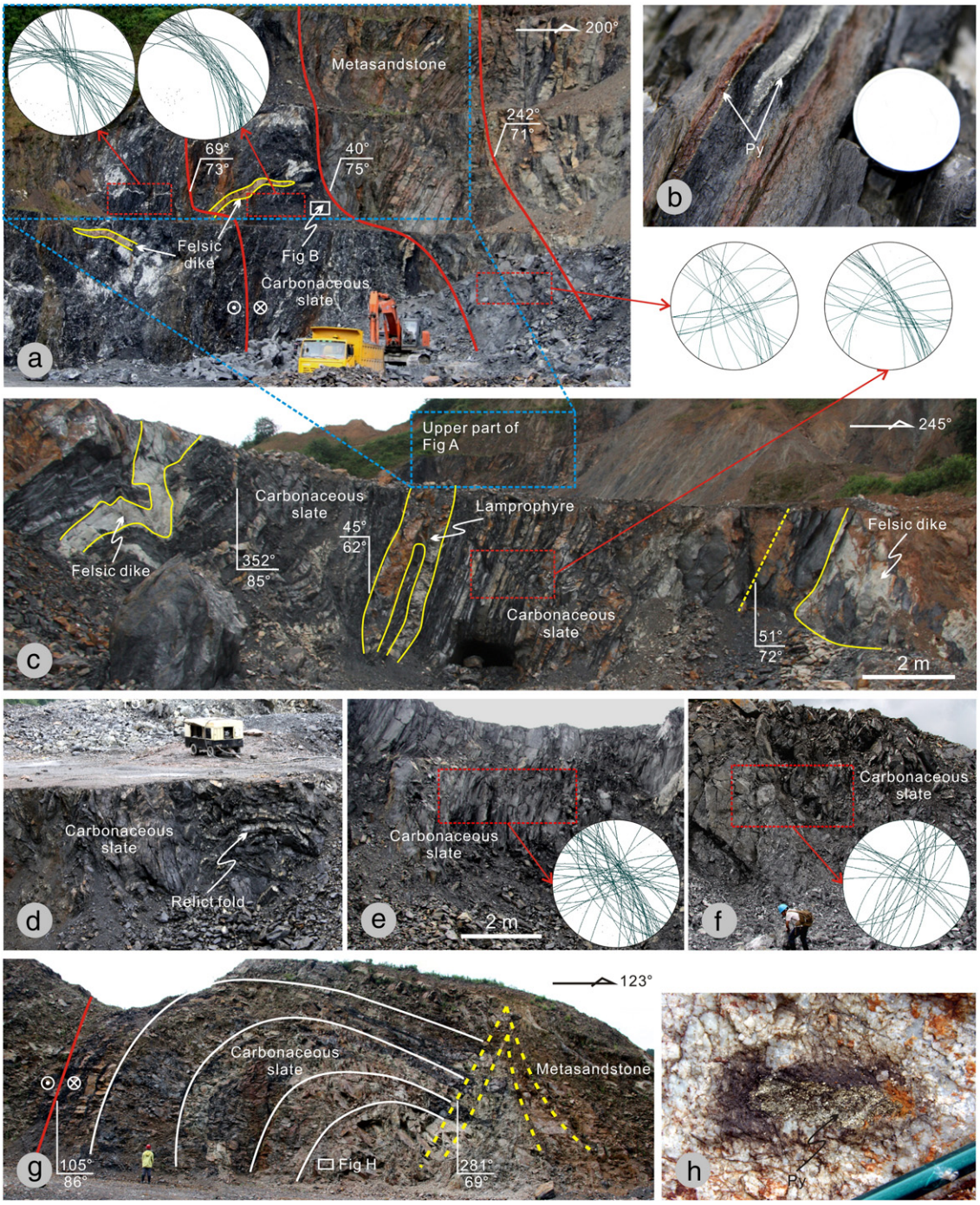

Fig. 4. Outcrop photographs of the Donggualin pit of the Zhenyuan ore deposit, SW China. (a) and (b) are the north wall of pit; (c), (d), (e) and (f) are in the central part of the pit; and (g) and (h) are in the south wall of pit. In (a), the wall is made up of meta-sandstone or carbonaceous slate slices bounded by NW-trending faults, the slates are reworked by dense joints shown by the joint statistics in (a) and sulfide deposit in the tensional spaces in joints illustrated in (b). In (c), the lamprophyre are contained in and controlled by the shear zone; the relict folds are present as shown in (c), (d), and (g); and the EW to NE-trending joints are observed, seen in the joint statistics in (a), (c), (e), and (f).

18.32–18.60, 15.67–15.72, and 38.74–38.96 (Table 3). The lead isotopes in the Laowangzhai cluster are almost identical to those of the Donggualin (Fig. 11), suggesting that the two clusters share the same metal sources. In the $^{208}Pb/^{204}Pb$ vs. $^{206}Pb/^{204}Pb$ diagram (Fig. 11b), most pyrite Pb isotope values in the two orebody clusters plot within the range of western Yunnan amphibolites, which represent one end-member of regional lower crust, and a few in the range of leucogranite. The leucogranite derived from the lower crust formed at a shallower level as compared to the regional amphibolites (Deng et al., 2014b). In the $^{207}Pb/^{204}Pb$ vs. $^{206}Pb/^{204}Pb$ diagram, the plots of the two clusters mainly overlap the range for western Yunnan amphibolites and leucogranite, and a few values fall towards the range of BSE (bulk silicate earth) (Fig. 11a). This shows that the ore materials were mainly derived from the lower crust with minor involvement of other sources.

5. Discussion

5.1. Controls on mineralization

The different gold abundances in different lithologies suggest that the mineralization is controlled by the lithology. This is consistent with the conclusion obtained from the enrichment of metallic elements

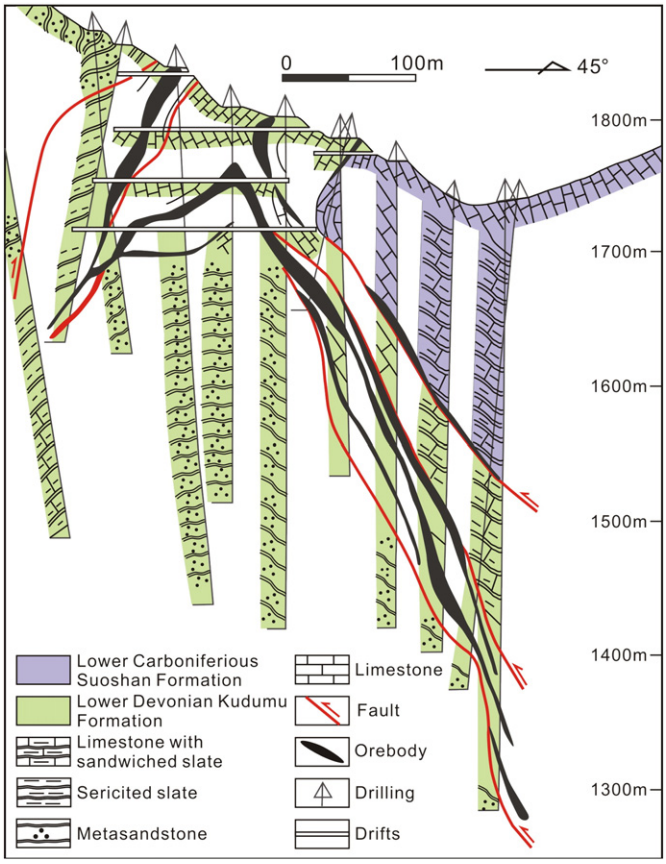

Fig. 5. Drill section (Line S0 shown in Fig. 3) in the Donggualin cluster of the Zhenyuan ore deposit, SW China.
Revised from BGMRYP (1993a).

in the analyzed samples of varied lithologies. Some of the host rocks are volumetrically more abundant than others in the orebody (Table 1). In the Donggualin orebody cluster, although the lamprophyre is volumetrically minor, it contains a large portion of the Au reserve. A variety of mechanisms have been proposed for the deposition of gold in the mafic igneous rocks, which include fluid–wall rock interaction (Palin and Xu, 2000), phase separation (Hodkiewicz et al., 2009; Palin and Xu, 2000), and mixing of fluids with contrasting redox states (Neumayr et al., 2008). The simple and uniform ore assemblage of sulfides displaying the absence of oxidized phases such as hematite and sulfate minerals, suggests a reduced redox state of the auriferous fluid. Therefore we interpret that the preferential mineralization in the lamprophyre is structurally controlled. Due to the high content of mica group minerals, lamprophyre has weaker mechanical strength than the surrounding meta-sedimentary rocks, and is more easily fractured during shearing, thereby facilitating the infiltration of ore fluids.

5.2. Source of ore fluids and materials

The two ore clusters, although with different orebody strikes, have a similar enriched element association, ore mineral assemblage, and Pb and S isotope compositions, which are indicative of a similar source. The results from Pb and S systematics in this study suggest that the ore-forming materials were mainly derived from lower crust with insignificant mixing from other sources.

Fluid inclusions from the auriferous quartz veins are dominantly NaCl–H_2O and H_2O–CO_2 with high CO_2 content (Bi et al., 1997; Burnard et al., 1999; Liang et al., 2011). Microthermometric measurements showed that the ore fluid is characterized by low salinity (6–8 wt.% NaCl eqv.) and moderate to low temperature (110–250 °C), which is different from the high temperature and salinity of primary magmatic hydrothermal ore deposits. The depth of the ore forming fluids calculated based on fluid inclusions is 0.37–3.74 km (Bi et al., 1997; He and Hu, 1996). The $\delta^{18}O$ ‰ (relative to SMOW) values of the ore fluids range from 1.6 to 11.77‰. The fluid δD_{H2O} (SMWD) values show a range of −50.3 to −105.1‰ (Hu et al., 1995; Liang et al., 2011). In the $\delta^{18}O_{H2O}$ versus δD_{H2O} diagram, the field of Zhenyuan extends from the range of metamorphic fluids to connate fluid because of the large variation in δD_{H2O} (Fig. 12). We interpret this as a reflection of isotope exchange as the metamorphic fluid migrated through the sedimentary rocks containing organic matter (Deng et al., 2014b).

The $\delta^{13}C$ of CO_2 in fluid inclusions from the auriferous quartz lies between −6.5 to −3.9‰, suggesting that the CO_2 in the ore fluid was mainly mantle-derived (Liang et al., 2011). The $^3He/^4He$ (0.17–0.73 Ra), $^{40}Ar/^{36}Ar$ (308–341), and ^3He/heat (0.1–0.8 × 10^{-12} cm^3 STP J^{-1}) of the ore fluids released by crushing pyrite grains (Burnard et al., 1999) showed that the gas in the fluid is a mixture of a mantle-derived and crust-derived components. The ore fluid was thus considered to be mainly metamorphic fluid, with minor involvement of mantle volatiles.

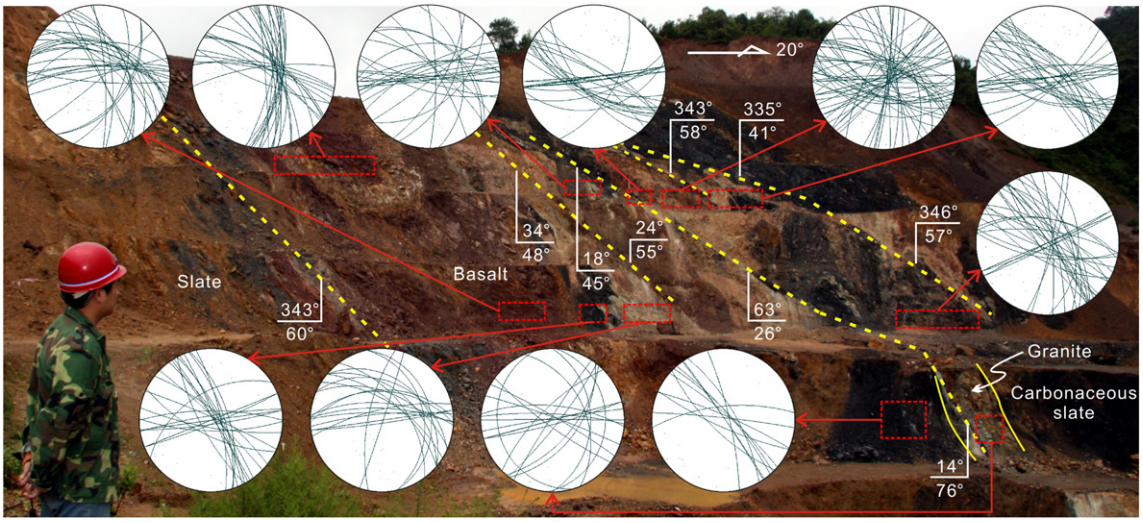

Fig. 6. Outcrop photographs of the Laowangzhai pit of the Zhenyuan ore deposit, SW China.

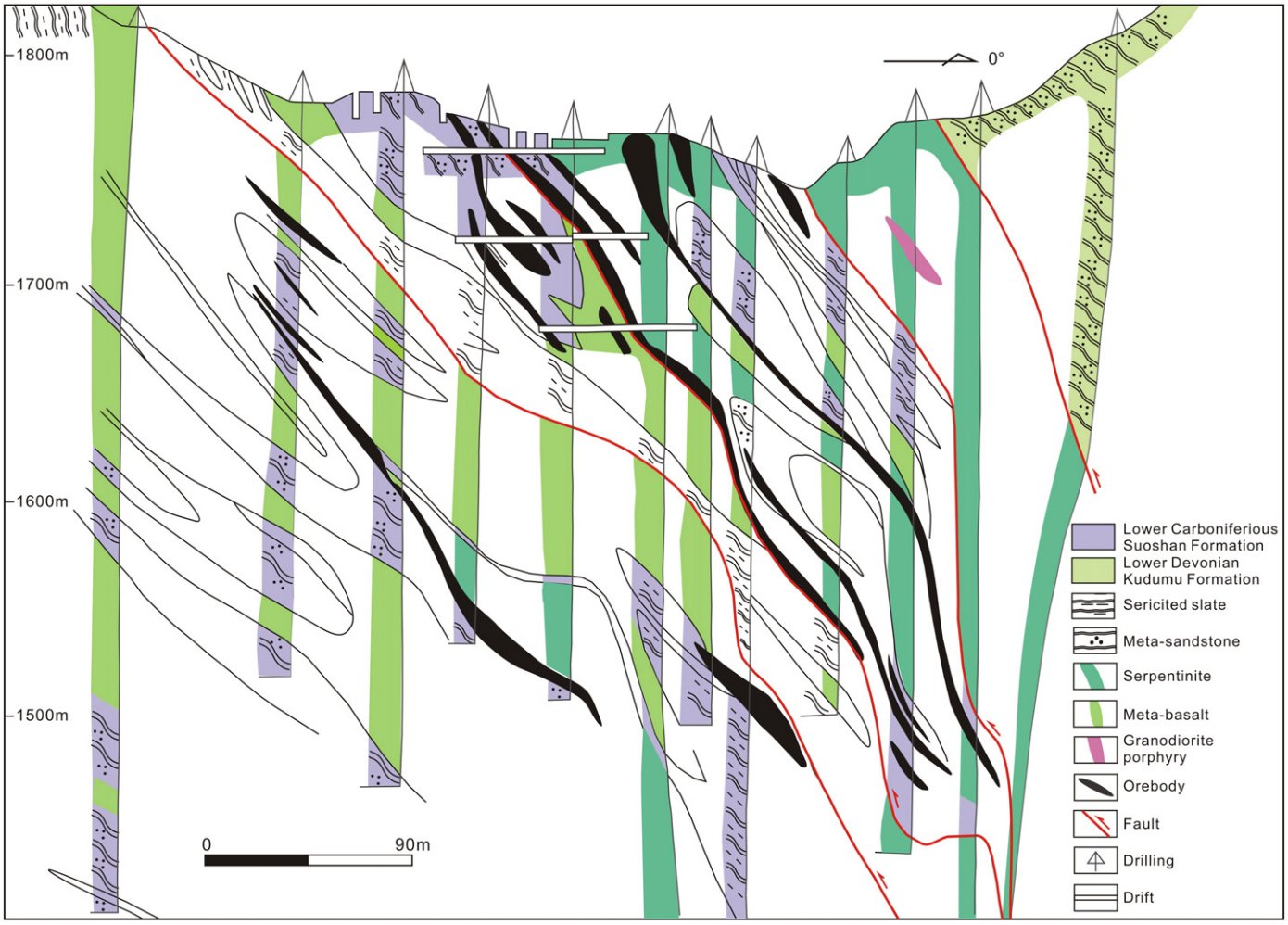

Fig. 7. Drill section (line 16 shown in Fig. 3) in the Laowangzhai cluster of the Zhenyuan ore deposit, SW China. Revised from BGMRYP (1993b).

5.3. Deposit genetic type and tectonic setting

The mineral assemblages and enrichment of elements in the ores, high CO_2 content in fluid inclusions, significant involvement of metamorphic fluid, and large contribution of lower crust to metals are compatible with the characteristics of orogenic gold deposits. Therefore the Zhenyan ore system can be categorized as orogenic type (Deng et al., 2014b; Goldfarb et al., 2001, 2014).

Available geochronological data from zircon U–Pb ages and whole rock or mica Ar–Ar ages show that the regional potassic magmatic rocks, including the felsic intrusion and mafic to felsic volcanic rocks, and the lamprophyre were emplaced from 44 to 32 Ma with a peak at 35 Ma (Fig. 13a). The magmatism has been correlated with mantle upwelling and crustal extension (Deng et al., 2014b; Lu et al., 2013). The porphyry ore deposits related to the potassic intrusions were formed in the same time span as inferred from the ages of ore-bearing porphyry and molybdenite (Fig. 13b). The shearing along the ASRRSZ occurred from 32 to 22 Ma (Cao et al., 2011; Sassier et al., 2009; Schärer et al., 1994; Tang et al., 2013; Zhang and Schärer, 1999) as indicated by zircon and monazite U–Pb ages from the leucogranite within the shear zone. The geochronological data show that the ASRRSZ shearing postdated the emplacement of the potassic igneous intrusive rocks

Table 1
Ore tonnage in different lithologies in the orebodies of the Zhenyuan gold deposit, SW China.

Orebody cluster	Laowangzhai			Donggualin		
Orebody no.	III_2	III_3	IV_1	SII_1	SII_2	$SIII_2$
Tonnage and grade	1,535,800 t 5.5 g/t Au	453,800 t 5.5 g/t Au	782,400 t 5.0 g/t Au	1,023,100 t 4.9 g/t Au	4,992,900 t 5.1 g/t Au	792,000 t 5.3 g/t Au
Ore tonnage distribution (%)						
Slate and limestone	15	27	39	46	30	3
Meta-sandstone	45	6	17	15	19	74
Granite	1	0	2	13	11	3
Lamprophyre	0	0	0	26	40	20
Meta-mafic to -ultramafic rocks	39	67	42	0	0	0

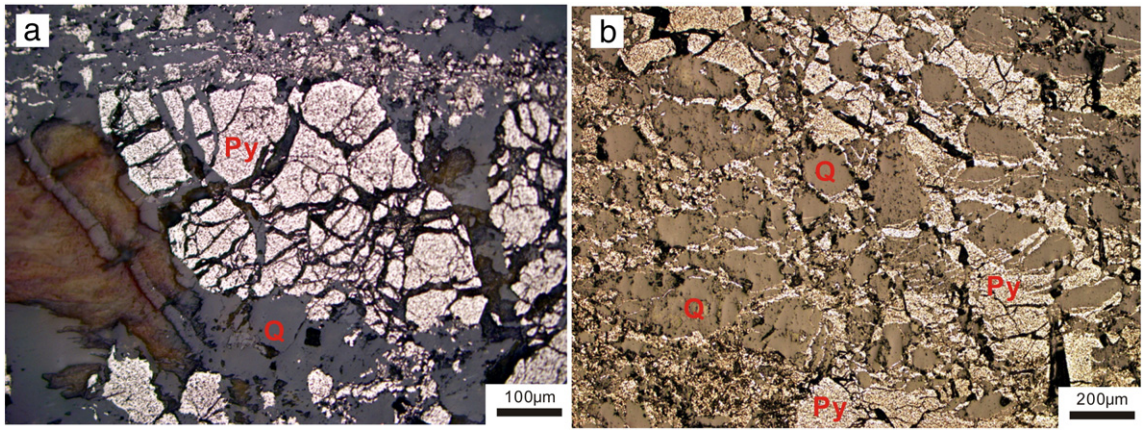

Fig. 8. Reflected light photomicrographs showing gold-bearing ores in the Zhenyuan ore deposit, SW China. (a) Brecciated pyrite in the Donggualin cluster; (b) crack-filling of the pyrite in the Donggualin cluster.

and lamprophyre (Fig. 13a). This temporal sequence is also confirmed by field relations in the Zhenyuan ore deposit, where the mineralized lamprophyre is controlled by the subsidiary shear zones.

An inverse isochron age at 26.4 ± 0.2 Ma from phlogopite in lamprophyre that intruded at ~33 Ma, in the Laowangzhai cluster was obtained and interpreted as the gold mineralization age (Wang et al., 2001a). The mineralization at Zhenyuan is broadly coincident with the culmination of the shearing along the ASRRSZ (Fig. 13). The ore fluid and metal source analysis in Zhenyuan suggests an episode of metamorphism from greenschist to amphibolite along the ASRRSZ occurred at ~27 Ma. The metamorphism is a response to the underthrust of continental lithosphere of South China block (Deng et al., 2014b). The significant involvement of mantle volatiles in the ore fluids suggests that mantle upwelling was most likely ongoing and the underthrust continental plate had not reached the lower-grade metamorphic unit west of the ASRRSZ, with the underthrusting of continental plate underneath inhibiting the mantle degassing (Gonnermann and Mukhopadhyay, 2009; Oppenheimer et al., 2011). The formation of the Zhenyuan gold deposit was considered to have occurred during the transition from mantle upwelling to continental underthrust. This tectonic setting distinguishes the Zhenyuan orogenic ore deposit from other classic orogenic gold deposits, which are mostly widely distributed in accreted terranes along the circum-Pacific margin (Bierlein and Crowe, 2000; Goldfarb et al., 1998, 2001, 2014).

Based on the structural and geochemical data, the formation of the Zhenyuan ore deposit can be envisaged as follows. In the waning stage of mantle upwelling or initiation of shearing, an array of nearly NS-trending faults was formed at ca. 32 Ma (Fig. 14a). At ca. 27 Ma, as the Simao block was largely rotated clockwise, the nearly NS-trending faults turned into NE- and ENE-orientation and might have been further reworked by the compression-shearing induced by block interaction. Due to the continental underthrust of South China block, the contemporary shearing along the ASRRSZ reached the climax, and the NW-trending subsidiary shear zone was developed to the west of ASRRSZ, cutting across the re-orientated NE- and ENE-faults (Fig. 14b). Meanwhile, the underthrusting caused the regional metamorphism releasing

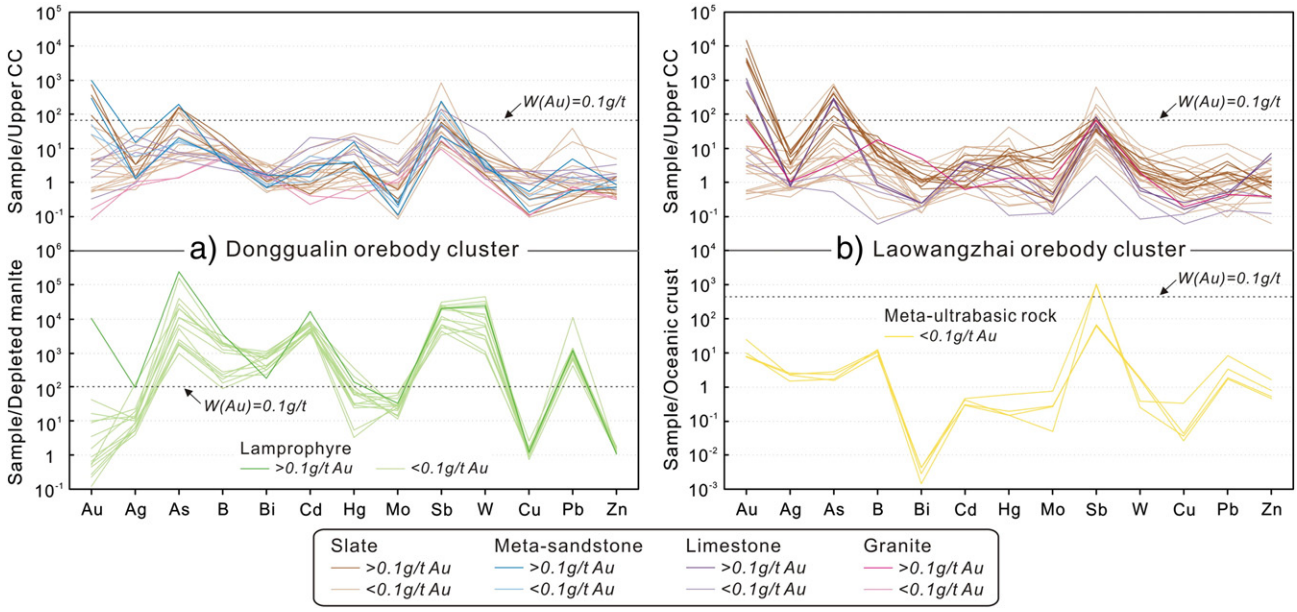

Fig. 9. Spiderdiagram of the trace elements of the Donggualin (a) and Laowangzhai (b) orebody clusters in the Zhenyuan ore deposit, SW China.
The normalized data of the upper continental crust (CC) is from Rudnick and Gao (2003), that of the depleted mantle is from Salters and Stracke (2004), and that of the oceanic crust from Taylor and Mclennan (1985).

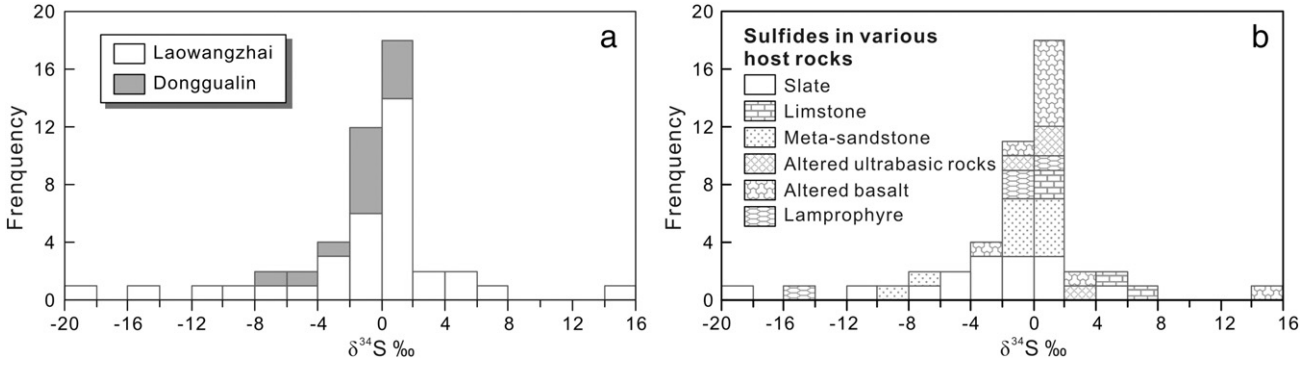

Fig. 10. Sulfur isotope compositions of sulfides in the Donggualin and Laowangzhai orebody clusters of the Zhenyuan ore deposit, SW China. The data are listed in Table 2.

gold-bearing metamorphic fluids. The fluid migrated westwards along the subsidiary shear zones, with input of volatiles discharged from the upwelled mantle. In the brittle fault network, the ore fluid deposited metals within various lithologies (Fig. 14c).

5.4. Regional metallogenesis

The Daping ore deposit, another shear zone-controlled one in the southern part of the low-grade metamorphic unit, formed at ~33 Ma according to the phlogopite Ar–Ar inverse isochron age (Fig. 13b). The metallogenesis is contemporary to the initial movement of the ASRRSZ (Sun et al., 2009). Ore minerals in this deposit include scheelite, pyrite, chalcopyrite, galena, bornite, and sphalerite. Fluid inclusions from the auriferous quartz show homogenization temperatures of 299–424 °C with a peak at 320–380 °C. Compared to the Zhenyuan ore deposit, the ore-forming fluids in Daping have higher temperature and greater depth of 5.1–12.9 km. The δD_{H2O} values of ore fluid are higher than those in the Zhenyuan, suggesting a more significant contribution from the metamorphic fluid in the Daping. The Daping ore deposit was suggested to have formed in a ductile–brittle transition zone (Sun et al., 2009). In contrast, the low temperature of ore fluid, limited depth, as well as the cataclastic structures in the Zhenyuan ore deposit suggest that metamorphic fluids migrated upwards along shear zones into the brittle domain in the shallow crust.

The compression due to the continental underthrust might have induced an increase of rock pressure and grade of metamorphism in crust, releasing Au-charged metamorphic fluid. The extensive development of shear zones facilitated the upward transportation of the ore fluids from depth. The gold deposits are located in subsidiary shear zone, and not in the first-order structures of ASRRSZ. It might be ascribed to that the ore fluids were expelled from the first-order shear zones due to the outward decrease in pressure.

Contemporary to the ASRRSZ, the NNW-trending shear zones of Chongshan and Gaoligong were formed in the Sanjiang region due to the India–Eurasia continent collision (Socquet and Pubellier, 2005). Although the kinematic features of these two shear zones are analogous to those of the ASRRSZ (Deng et al., 2014b), there is no noticeable mineralization along these two zones. The barren nature of the two shear

Table 2
Sulfur isotopes (CDT ‰) in the ore pyrites from the Donggualin and Laowangzhai districts in the Zhenyuan deposit, SW China.

Sample no.	Mineral	Sample locations	Host lithology	$\delta^{34}S$ ‰	Data sources	Sample no.	Mineral	Sample locations	Host lithology	$\delta^{34}S$ ‰	Data sources
L04-1	Pyrite	Laowangzhai	Slate	−0.9	This paper	LTZ-34	Pyrite	Laowangzhai	Meta-sandstone	−8.38	Hu et al. (1995)
L04-2	Pyrite	Laowangzhai	Slate	5.3	This paper	L02-1	Pyrite	Laowangzhai	Limestone	0.6	This paper
L04-3	Pyrite	Laowangzhai	Slate	−11.2	This paper	LTZ-26	Pyrite	Donggualin	Limestone	0.57	Hu et al. (1995)
L04-4	Pyrite	Laowangzhai	Slate	0.1	This paper	LTZ-36	Pyrite	Laowangzhai	Limestone	4.04	Hu et al. (1995)
L04-5	Pyrite	Laowangzhai	Slate	−7.5	This paper	LTZ-37	Pyrite	Laowangzhai	Limestone	6.7	Hu et al. (1995)
L07-1	Pyrite	Laowangzhai	Slate	−3.8	This paper	LTZ-3	Wolfsbergite	Laowangzhai	Altered ultrabasic rocks	0.51	Hu et al. (1995)
L08-2	Pyrite	Laowangzhai	Slate	−3.2	This paper	LTZ-9	Pyrite	Laowangzhai	Altered ultrabasic rocks	3.6	Hu et al. (1995)
L12-7	Pyrite	Laowangzhai	Slate	−4.1	This paper	LTZ-16	Pyrite	Laowangzhai	Altered ultrabasic rocks	0.48	Hu et al. (1995)
L53-1	Pyrite	Laowangzhai	Slate	−19.1	This paper	L189	Pyrite	Laowangzhai	Altered ultrabasic rocks	−1.63	Hu et al. (1995)
D04-1	Pyrite	Donggualin	Slate	−1.5	This paper	I139	Pyrite	Laowangzhai	Altered basalt	1.2	Hu et al. (1995)
D08-8	Pyrite	Donggualin	Slate	−2.8	This paper	I159	Pyrite	Laowangzhai	Altered basalt	2.7	Hu et al. (1995)
D14-6	Pyrite	Donggualin	Slate	1.8	This paper	L178	Pyrite	Laowangzhai	Altered basalt	−0.36	Hu et al. (1995)
LTZ-7	Pyrite	Laowangzhai	Slate	−0.37	Hu et al. (1995)	LTZ-10	Pyrite	Laowangzhai	Altered basalt	1.89	Hu et al. (1995)
LTZ-8	Pyrite	Donggualin	Slate	−5.57	Hu et al. (1995)	LTZ-12	Pyrite	Laowangzhai	Altered basalt	0.81	Hu et al. (1995)
LTZ-11	Pyrite	Laowangzhai	Slate	1.34	Hu et al. (1995)	LTZ-13	Pyrite	Laowangzhai	Altered basalt	0.2	Hu et al. (1995)
LTZ-1	Wolfsbergite	Donggualin	Meta-sandstone	0.68	Hu et al. (1995)	LTZ-15	Pyrite	Laowangzhai	Altered basalt	15.41	Hu et al. (1995)
LTZ-2	Pyrite	Donggualin	Meta-sandstone	0.18	Hu et al. (1995)	LTZ-17	Pyrite	Laowangzhai	Altered basalt	1.13	Hu et al. (1995)
LTZ-4	Pyrite	Donggualin	Meta-sandstone	−0.86	Hu et al. (1995)	LTZ-20	Pyrite	Laowangzhai	Altered basalt	1.3	Hu et al. (1995)
LTZ-8	Pyrite	Laowangzhai	Meta-sandstone	−0.54	Hu et al. (1995)	LTZ-21	Pyrite	Laowangzhai	Altered basalt	−2.37	Hu et al. (1995)
LTZ-14	Pyrite	Laowangzhai	Meta-sandstone	1.89	Hu et al. (1995)	A279	Pyrite	Laowangzhai	Lamprophyre	0.21	Hu et al. (1995)
LTZ-22	Pyrite	Laowangzhai	Meta-sandstone	0.08	Hu et al. (1995)	L11-4	Pyrite	Laowangzhai	Lamprophyre	−14.5	This paper
LTZ-23	Pyrite	Donggualin	Meta-sandstone	−0.1	Hu et al. (1995)	LTZ-2	Wolfsbergite	Donggualin	Lamprophyre	−0.44	Hu et al. (1995)
LTZ-27	Pyrite	Donggualin	Meta-sandstone	−6.79	Hu et al. (1995)	LTZ-29	Pyrite	Donggualin	Lamprophyre	−0.12	Hu et al. (1995)
LTZ-33	Wolfsbergite	Donggualin	Meta-sandstone	−0.62	Hu et al. (1995)						

Table 3
Lead isotopes in pyrite from the Zhenyuan deposit, China.

Number	Location	$^{206}Pb/^{204}Pb$	$^{207}Pb/^{204}Pb$	$^{208}Pb/^{204}Pb$
L02-2	Laowangzhai	18.01	15.60	38.39
L04-1	Laowangzhai	18.64	15.72	39.04
L04-2	Laowangzhai	18.57	15.74	38.98
L04-3	Laowangzhai	18.64	15.74	39.08
L04-4	Laowangzhai	18.76	15.73	39.24
L04-5	Laowangzhai	18.62	15.72	39.10
L07-1	Laowangzhai	18.47	15.70	38.88
L08-2	Laowangzhai	18.31	15.70	38.48
L11-4	Laowangzhai	18.10	15.62	38.50
L12-2	Laowangzhai	18.43	15.71	38.71
L12-6	Laowangzhai	17.16	15.38	37.47
L12-7	Laowangzhai	18.49	15.70	38.88
L53-1	Laowangzhai	18.54	15.72	38.91
D03-2	Donggualin	18.57	15.71	38.93
D04-1	Donggualin	18.54	15.70	38.89
D08-8	Donggualin	18.60	15.72	38.96
D14-6	Donggualin	18.32	15.67	38.74

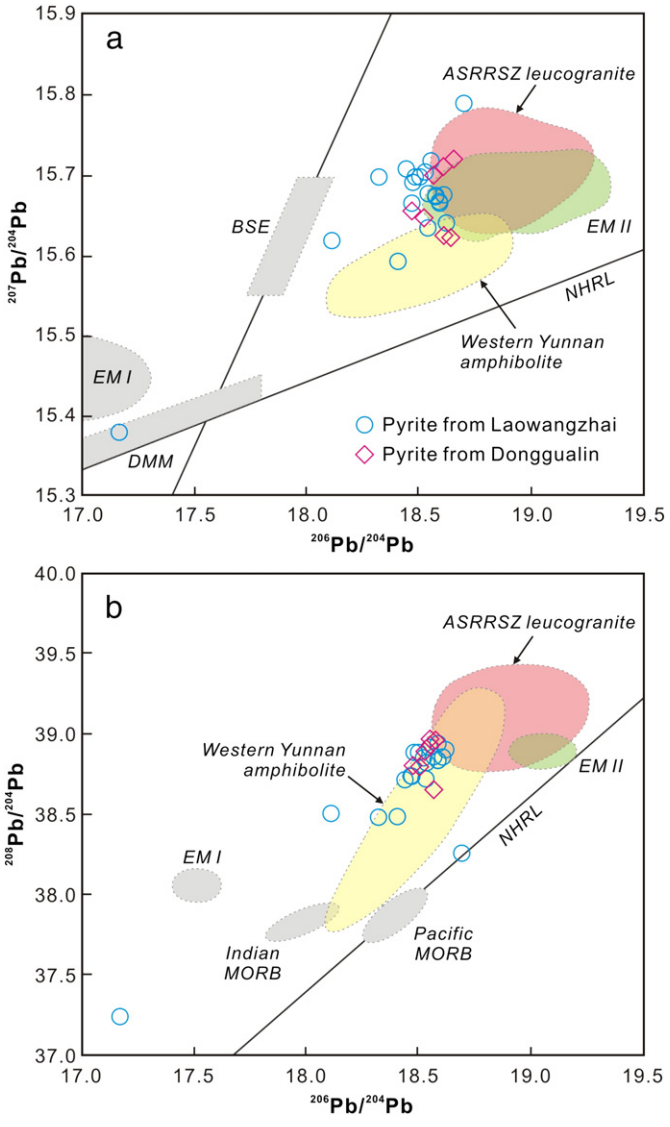

Fig. 11. Lead isotope compositions of sulfides from the Donggualin and Laowangzhai orebody clusters of the Zhenyuan ore deposit, SW China. (a) $^{207}Pb/^{204}Pb$ vs. $^{206}Pb/^{204}Pb$. (b) $^{208}Pb/^{204}Pb$ vs. $^{206}Pb/^{204}Pb$. The diagram is from Lu et al. (2013). Mantle source reservoirs BSE, MORB, DMM, EM I, and EM II are from Zindler and Hart (1986). Indian MORB and Pacific MORB are after Guo et al. (2005). The Northern Hemisphere Reference Line (NHRL) is from Hart (1984). Data for leucogranite are from Zhang and Schärer (1999) and those for amphibolite xenoliths in the potassic felsic intrusion are from Deng et al. (1998) and Zhao et al. (2004).

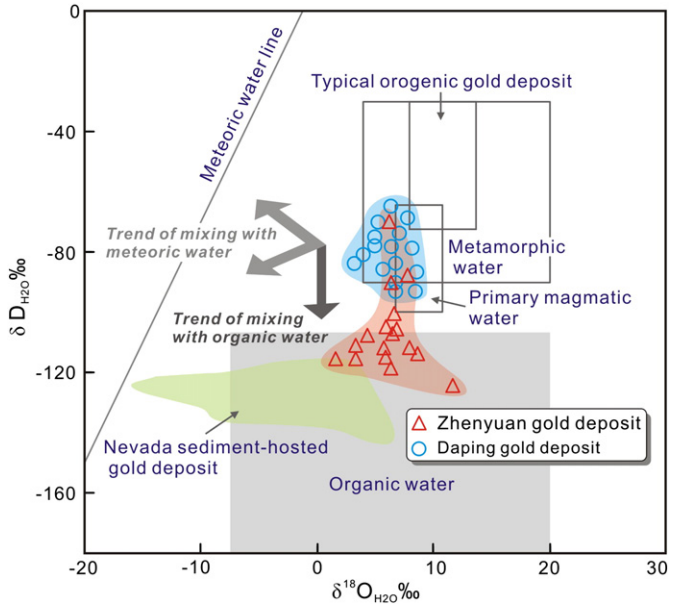

Fig. 12. δD and $\delta^{18}O$ isotope compositions of auriferous fluid in the orogenic Au deposit in the Ailaoshan tectonic belt, SW China. The $\delta^{18}O_{H2O}$ ‰ (relative to SMOW) values of the ore-forming fluids are calculated by the values of auriferous quartz based on the isotopic fractionation equation in equilibrium, and δD_{H2O} (SMWD) values of the water were analyzed directly from the fluid inclusions.
The magmatic, metamorphic, and organic fields are from Sheppard (1986). The field for orogenic gold deposit is from Goldfarb et al. (2004) and that for the Navada gold deposit is from Field and Fifarek (1985) Age data for the Zhenyuan ore deposit are from Hu et al. (1995) and Liang et al. (2011), and those in the Daping ore deposit from Sun et al. (2009).

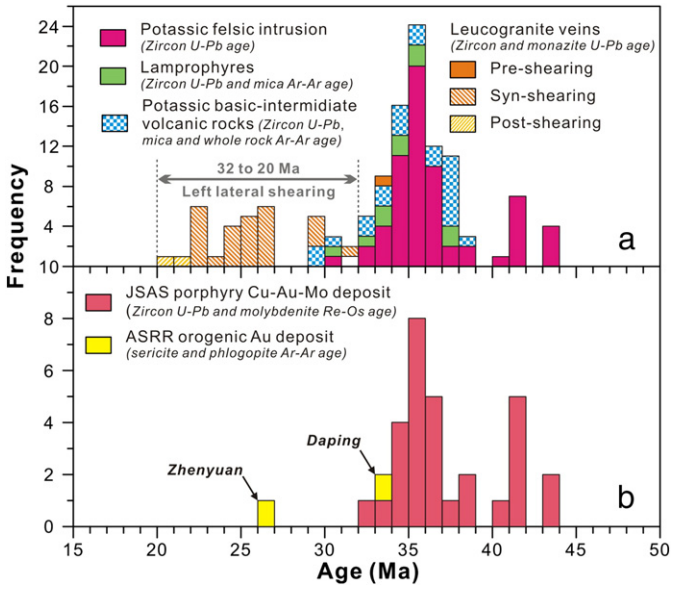

Fig. 13. Age histogram of Cenozoic igneous rocks, porphyry Cu–Au–Mo deposit, and orogenic Au deposit along the Jinshajiang–Ailaoshan belt, SW China. The time for the potassic magmatism including felsic intrusion, mafic–intermediate volcanic rocks and lamprophyre is 44–32 Ma. The subsequent ductile left-lateral shearing along Ailaoshan–Red River shear zone is limited in 32–22 Ma by the age of the leucogranite within the shear zone.
The emplacement ages of the igneous rocks are from Cao et al. (2011), Chung et al. (1997), Flower et al. (2013), Guo et al. (2005, 2006), He et al. (2013), Huang et al. (2010), Jia et al. (2013), Jiang et al. (2006), Leloup et al. (2001), Liang et al. (2006, 2007, 2008, 2009), Lu et al. (2012), Sassier et al. (2009), Schärer et al. (1994), Spurlin et al. (2005), Tang et al. (2013), Wang et al. (2001b, 2003, 2009) and Zhang and Schärer (1999); and the formation ages of the ore deposits are the same as Fig. 1.

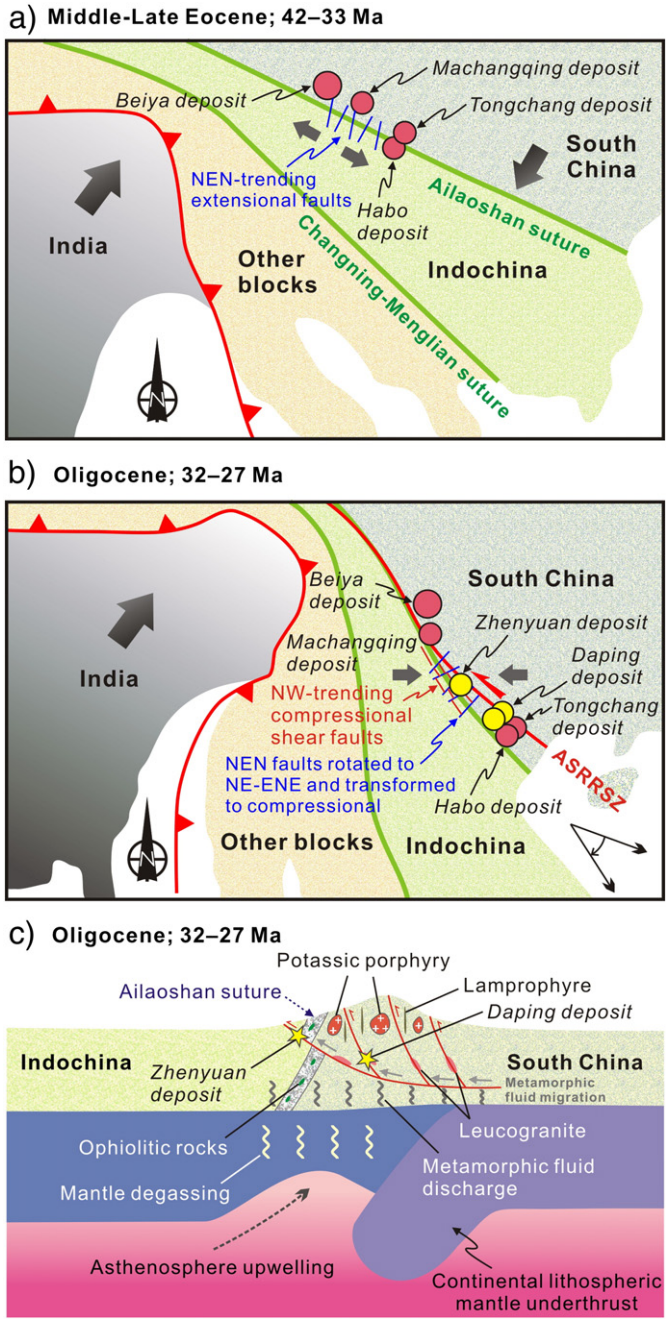

Fig. 14. Tectonic models for the orogenic Au deposits in the Ailaoshan tectonic belt, SW China. (a) In the waning stage of mantle upwelling and initiation of ASRRSZ shearing, an array of nearly NS-trending faults formed at ca. 32 Ma; (b) the nearly NS-trending faults were afterwards re-oriented and further cut by the new NW-trending shear zones subsidiary to ASRRSZ; (c) the underthrusting of South China block triggered the release of gold-charged metamorphic fluid at ~27 Ma. The fluid migrated westwards along the subsidiary shear zones, with input of mantle gas discharged in the waning stage of the mantle upwelling, forming the orogenic gold ore deposits, e.g., Zhenyuan and Daping, at different depths.

zones is most likely related to the absence of a continental underthrust, which is considered as the driving force for ore fluid formation.

6. Conclusions

It is proposed the NE- and ENE-trending faults controlling the mineralization in Laowangzhai ore cluster primarily formed as nearly NS-trending zones in response to the crustal extension or the following initial shearing at ~32 Ma. Subsequently, due to the rotation and lateral extrusion of Indochina block, these nearly NS-trending zones were rotated clockwise to the current orientation and were further cut by the NW-trending shear zones. The later NW-trending faults controlled the mineralization in the Laowangzhai orebody cluster.

The ore mineral assemblages, enrichment in metallic elements, and S–Pb isotopic compositions are generally comparable in the two clusters, suggesting that they share a coeval and analogous ore-forming process. The S and Pb isotopes, in combination with the previously published H–O–He–Ar isotopic data, indicate that the ore fluid was mainly composed of metamorphic fluid with important input of mantle volatiles. The ore-forming metals were dominantly derived from the lower crust.

The Zhenyuan ore deposit is classified as orogenic type, with a unique tectonic setting of continental underthrust and concomitant mantle upwelling. The underthrusting of South China lithosphere was the potential trigger for the release of the Au-charged metamorphic fluid. The fluid was further channeled by subsidiary shear zones forming several orogenic gold deposits at various depths to the west of the Ailaoshan–Red River shear zone.

Supplementary data to this article can be found online at http://dx.doi.org/10.1016/j.oregeorev.2014.08.002.

Acknowledgements

The constructive comments and careful revisions from the editor-in-chief F.M. Pirajno, associate editor, and two reviewers are greatly appreciated. We sincerely thank the leaders and engineers in the Zhenyuan gold deposit for their support during our fieldwork. This work was supported by the National Key Basic Research Development Program (2009CB421008), Planning Project of China Geological Survey (12120114039701)

References

Belshaw, N.S., Freedman, P.A., O'Nions, R.K., Frank, M., Guo, Y., 1998. A new variable dispersion double-focusing plasma mass spectrometer with performance illustrated for Pb isotopes. Int. J. Mass Spectrom. 181, 51–58.

BGMRYP (Bureau of Geology and Mineral Resources of Yunnan Province), 1993a. Exploration Report of the Donggualin Orebody Cluster, Zhenyuan Deposit, Yunnan Province, (in Chinese).

BGMRYP (Bureau of Geology and Mineral Resources of Yunnan Province), 1993b. Exploration Report of the Laowangzhai Orebody Cluster, Zhenyuan Deposit, Yunnan Province, (in Chinese).

Bi, X.W., Hu, R.Z., He, M.Y., 1996. ESR dating of Ailaoshan gold metallogenic belt and geologic significance. Chin. Sci. Bull. 41, 1546–1549.

Bi, X.W., Hu, R.Z., He, M.Y., 1997. Characteristics of ore-forming fluid of three gold deposits in Aialaoshan gold metallogenic belt. Acta Mineral. Sin. 17, 435–441 (in Chinese with English abstract).

Bierlein, F.P., Crowe, D.E., 2000. Phanerozoic orogenic lode gold deposits. In: Hagemann, S.G., Brown, P.E. (Eds.), Gold in Ž. Society of Economic Geologists Reviews in Economic Geology. 13, pp. 103–139.

Burnard, P.G., Hu, R.Z., Turner, G., Bi, X.W., 1999. Mantle crustal and atmospheric noble gases in Ailaoshan gold deposits, Yunnan Province, China. Geochim. Cosmochim. Acta 63, 1595–1604.

Cao, S.Y., Liu, J.L., Leiss, B., Neubauer, F., Genser, J., Zhao, C.Q., 2011. Oligo-Miocene shearing along the Ailao Shan–Red River shear zone: constraints from structural analysis and zircon U–Pb geochronology of magmatic rocks in the Diancang Shan massif, SE Tibet, China. Gondwana Res. 19, 975–993.

Chung, S.L., Lee, T.Y., Lo, C.H., Wang, P.L., Chen, C.Y., Yem, N.T., Hoa, T.T., Wu, G.Y., 1997. Intraplate extension prior to continental extrusion along the Ailaoshan–Red River shear zone. Geology 25, 311–314.

Deng, W.M., Huang, X., Zhong, D.L., 1998. Petrological characteristics and genesis of Cenozoic alkali-rich porphyry in West Yunnan, China. Sci. Geol. Sin. 33, 412–425 (in Chinese with English abstract).

Deng, J., Wang, Q.F., Yang, L.Q., Wang, Y.R., Gong, Q.J., Liu, H., 2010a. Delineation and exploration of geochemical anomalies using fractal models in the Heqing area, Yunnan Province, China. J. Geochem. Explor. 105, 95–105.

Deng, J., Yang, L.Q., Ge, L.S., Yuan, S.S., Wang, Q.F., Zhang, J., Gong, Q.J., Wang, C.M., 2010b. Character and post-ore changes, modifications and preservation of Cenozoic alkali-rich porphyry gold metallogenic system in western Yunnan, China. Acta Petrol. Sin. 26, 1633–1645 (in Chinese with English abstract).

Deng, J., Yang, L.Q., Wang, C.M., 2011. Research advances of superimposed orogenesis and metallogenesis in the Sanjiang Tethys. Acta Petrol. Sin. 27, 2501–2509 (in Chinese with English abstract).

Deng, J., Wang, Q.F., Li, G.J., Li, C.S., Wang, C.M., 2014a. Tethys tectonic evolution and its bearing on the distribution of important mineral deposits in the Sanjiang region, SW China. Gondwana Res. 26, 419–437.
Deng, J., Wang, Q.F., Li, G.J., Santosh, M., 2014b. Cenozoic tectono-magmatic and metallogenic processes in the Sanjiang region, southwestern China. Earth-Sci. Rev. http://dx.doi.org/10.1016/j.earscirev.2014.05.015.
Field, C.W., Fifarek, R.H., 1985. Light stable-isotopic systematics in the epithermal environment. Rev. Econ. Geol. 2, 99–128.
Flower, M.F.J., Hoàng, N., Lo, C.H., Chí, C.T., Cu'ò'ng, N.Q., Liu, F.T., Deng, J.F., Mo, X.X., 2013. Potassic magma genesis and the Ailao Shan–Red River fault. J. Geodyn. 69, 84–105.
Goldfarb, R.J., Phillips, G.N., Nokleberg, W.J., 1998. Tectonic setting of synorogenic gold deposits of the Pacific Rim. Ore Geol. Rev. 13, 185–218.
Goldfarb, R.J., Groves, D.I., Gardoll, S., 2001. Orogenic gold and geologic time: a global synthesis. Ore Geol. Rev. 18, 1–75.
Goldfarb, R.J., Ayuso, R., Miller, M.L., Ebert, S.W., Marsh, E.E., Petsel, S.A., Miller, L.D., Bradley, D., Johnson, C., McClelland, W., 2004. The late Cretaceous Donlin Creek gold deposit, Southwestern Alaska: controls on epizonal ore formation. Econ. Geol. 99, 643–671.
Goldfarb, R.J., Taylor, R.D., Collins, G.S., Goryachev, A., Orlandini, F., 2014. Phanerozoic continental growth and gold metallogeny of Asia. Gondwana Res. 25, 48–102.
Gonnermann, H.M., Mukhopadhyay, S., 2009. Preserving noble gases in a convecting mantle. Nature 459, 560–564.
Guo, Z.F., Hertogen, J., Liu, J.Q., Pasteels, P., Boven, A., Punzalan, L., He, H.Y., Luo, X.J., Zhang, W.H., 2005. Potassic magmatism in Western Sichuan and Yunnan Provinces, SE Tibet, China: petrological and geochemical constraints on petrogenesis. J. Petrol. 46, 33–78.
Guo, L.G., Liu, Y.P., Xu, W., Zhang, X.C., Qin, K.Z., Li, T.S., Shi, Y.R., 2006. Constraints to the mineralization age of the Yulong porphyry copper deposit from SHRIMP U–Pb zircon data in Tibet. Acta Petrol. Sin. 21, 1009–1016 (in Chinese with English abstract).
Hart, S.R., 1984. A large-scale isotope anomaly in the southern hemisphere mantle. Nature 309, 753–757.
He, M.Y., Hu, R.Z., 1996. Source and characteristics of ore-bearing hydrothermal solution in Laowangzhai gold deposit field. Bull. Mineral. Petrol. Geochem. 15, 36–39 (in Chinese with English abstract).
He, W.Y., Mo, X.X., Yu, X.H., He, Z.H., Dong, G.C., Liu, X.B., Su, G.S., Huang, X.F., 2013. Zircon U–Pb and molybdenite Re–Os dating for the Beiya gold–polymetallic deposit in the western Yunnan Province and its geological significance. Acta Petrol. Sin. 29, 1301–1310 (in Chinese with English abstract).
Hodkiewicz, P.F., Groves, D.I., Davidson, G.J., Weinberg, R.F., Hagemann, S.G., 2009. Influence of structural setting on sulphur isotopes in Archean orogenic gold deposits, Eastern Goldfields Province, Yilgarn, Western Australia. Mineral. Deposita 44, 129–150.
Hou, Z.Q., Cook, N.J., 2009. Metallogenesis of the Tibetan collisional orogen: a review and introduction to the special issue. Ore Geol. Rev. 36, 2–24.
Hou, Z.Q., Zeng, P.S., Gao, Y.F., Du, A.D., Fu, D.M., 2006. Himalayan Cu–Mo–Au mineralization in the eastern Indo-Asian collision zone: constraints from Re–Os dating of molybdenite. Mineral. Deposita 41, 33–45.
Hou, Z.Q., Zaw, K., Pan, G.T., Mo, X.X., Xu, Q., Hu, Y.Z., Li, X.Z., 2007. Sanjiang Tethyan metallogenesis in S.W. China: tectonic setting, metallogenic epochs and deposit types. Ore Geol. Rev. 31, 48–87.
Hu, Y.Z., Tang, S.C., Wang, H.P., 1995. Geology of Gold Deposits in Ailaoshan. Geological Press, Beijing, pp. 1–273 (in Chinese).
Hu, R.Z., Bi, X.W., He, M.Y., Liu, B.G., Turner, G., Burnard, P.G., 1998. Mineralizer constraint on gold mineralization of Ailaoshan gold belt. Sci. China Ser. D Earth Sci. 41 (Suppl.), 74–82.
Huang, Z.L., Liu, C.Q., Yang, H.L., Xu, C., Han, R.S., Xiao, H.Y., Zhang, B., Li, W.B., 2002. Geochemistry of lamprophyres in Laowangzhai gold deposits, Yunnan Province, China: implication for its characteristics of source region. Geochem. J. 39, 91–112.
Huang, X.L., Niu, Y., Xu, Y.G., Chen, L.L., Yang, Q.J., 2010. Mineralogical and geochemical constraints on the petrogenesis of post-collisional potassic and ultrapotassic rocks from western Yunnan, SW China. J. Petrol. 51, 1617–1654.
Jia, L.Q., Mo, X.X., Dong, G.C., Xu, W.Y., Wang, L., Guo, X.D., Wang, Z.H., Wei, S.G., 2013. Genesis of lamprophyres from Machangqing, western Yunnan: constraints from geochemistry, geochronology and Sr–Nd–Pb–Hf isotopes. Acta Petrol. Sin. 29, 1247–1260 (in Chinese with English abstract).
Jiang, Y.H., Jiang, S.Y., Ling, H.F., Dai, B.Z., 2006. Low-degree melting of a metasomatized lithospheric mantle for the origin of Cenozoic Yulong monzogranite-porphyry, east Tibet: geochemical and Sr–Nd–Pb–Hf isotopic constraints. Earth Planet. Sci. Lett. 241, 617–633.
Lai, C.K., Meffre, S., Crawford, A.J., Zaw, K., Halpin, A., Xue, C.D., Salam, A., 2014a. The Central Ailaoshan ophiolite and modern analogs. Gondwana Res. 26, 75–88.
Lai, C.K., Meffre, S., Crawford, A.J., Zaw, K., Xue, C.D., Halpin, J.A., 2014b. The Western Ailaoshan Volcanic Belts and their SE Asia connection: a new tectonic model for the Eastern Indochina Block. Gondwana Res. 26, 52–74.
Lee, T.Y., Lawver, L.A., 1995. Cenozoic plate reconstruction of Southeast Asia. Tectonophysics 251, 85–138.
Leloup, P.H., Lacassin, R., Tapponnier, P., Scharer, U., Zhong, D.L., Liu, X.H., Zhang, L.C., Ji, S.C., Trinh, P.T., 1995. The Ailao Shan–Red River shear zone (Yunnan, China), tertiary transform boundary of Indochina. Tectonophysics 251, 3–84.
Leloup, P.H., Arnaud, N., Lacassin, R., Kienast, J.R., Harrison, T.M., Phan Trong, T.T., Replumaz, A., Tapponnier, P., 2001. New constraints on the structure, thermochronology, and timing of the Ailao Shan–Red River shear zone, SE Asia. J. Geophys. Res. 106, 6683–6732.
Li, G.J., Wang, Q.F., Yu, L., Hu, Z.C., Ma, N., Huang, Y.H., 2013a. Closure time of the Ailaoshan Paleo-Tethys Ocean: constraints from the zircon U–Pb dating and geochemistry of the Late Permian granitoids. Acta Petrol. Sin. 29, 3883–3900 (in Chinese with English abstract).
Li, G.J., Wang, Q.F., Wang, J.Q., Fang, Q.L., 2013b. Geological and geochemical characteristics of the Huangshilao Stratabound gold deposit in the Tongguanshan Orefield, Tongling, East-Central China. Resour. Geol. 63, 141–154.
Liang, H.Y., Campbell, I.H., Allen, C., Sun, W.D., Liu, C.Q., Yu, H.X., Xie, Y.W., Zhang, Y.Q., 2006. Zircon Ce^{4+}/Ce^{3+} ratios and ages for Yulong ore-bearing porphyries in eastern Tibet. Mineral. Deposita 41, 152–159.
Liang, H.Y., Campbell, I.H., Allen, C.M., Sun, W.D., Yu, H.X., Xie, Y.W., Zhang, Y.Q., 2007. The age of the potassic alkaline igneous rocks along the Ailao Shan–Red River shear zone: implications for the onset age of left-lateral shearing. J. Geol. 115, 231–242.
Liang, H.Y., Mo, J.H., Sun, W.D., Yu, H.X., Zhang, Y.Q., Allen, C.M., 2008. Study on the duration of the ore-forming system of the Yulong giant porphyry copper deposit in eastern Tibet, China. Acta Petrol. Sin. 24, 2352–2358 (in Chinese with English abstract).
Liang, H.Y., Mo, J.H., Sun, W.D., Zhang, Y.Q., Zeng, T., Hu, G.Q., Allen, C.M., 2009. Study on geochemical composition and isotope ages of the Malasongduo porphyry associated with Cu–Mo mineralization. Acta Petrol. Sin. 25, 385–392 (in Chinese with English abstract).
Liang, Y.H., Sun, X.M., Shi, G.Y., Hu, B.M., Zhou, F., Wei, H.X., Mo, R.W., 2011. Ore-forming fluid geochemistry and genesis of Laowangzhai large scale orogenic gold deposit in Ailaoshan gold belt, Yunnan Province, China. Acta Petrol. Sin. 27, 2533–2540 (in Chinese with English abstract).
Liu, F.T., Liu, J.H., Zhong, D.L., He, J.K., You, Q.Y., 2000. The subducted slab of Yangtze continental block beneath the Tethyan orogen in western Yunnan. Chin. Sci. Bull. 45, 466–472.
Liu, J.L., Tang, Y., Tran, M.D., Cao, S.Y., Zhao, L., Zhang, Z.C., Zhao, Z.D., Chen, W., 2012. The nature of the Ailao Shan–Red River (ASRR) shear zone: constraints from structural, microstructural and fabric analyses of metamorphic rocks from the Diancang Shan, Ailaoshan and Day Nui Con Voi massifs. Earth Planet. Sci. Lett. 47, 231–251.
Lu, Y.J., Kerrich, R., Cawood, P.A., McCuaig, C.T., Hart, C.J.R., Li, Z.X., Hou, Z.Q., Bagas, L., 2012. Zircon SHRIMP U–Pb geochronology of potassic felsic intrusions in western Yunnan, SW China: constraints on the relationship of magmatism to the Jinsha suture. Gondwana Res. 22, 737–747.
Lu, Y.J., Kerrich, R., Kemp, A.I.S., Mccuaig, T.C., Hou, Z.Q., Hart, C.J., Li, Z.X., Cawood, P.A., Bagasi, L., Yang, Z.M., Cliff, J., Belousov, E.A., Jourdan, F., Evans, N.J., 2013. Intracontinental Eocene–Oligocene porphyry Cu mineral systems of Yunnan, Western Yangtze Craton, China: compositional characteristics, sources, and implications for continental collision metallogeny. Econ. Geol. 108, 1541–1576.
Metcalfe, I., 2011. Tectonic framework and Phanerozoic evolution of Sundaland. Gondwana Res. 19, 3–21.
Mo, X.X., Lu, F.X., Shen, S.Y., 1993. Sanjiang Tethyan Volcanism and Related Mineralization. Geological Publishing House, Beijing, pp. 1–267 (in Chinese).
Neumayr, P., Walshe, J., Hagemann, S., Petersen, K., Roache, A., Frikken, P., Horn, L., Halley, S., 2008. Oxidized and reduced mineral assemblages in greenstone belt rocks of the St. Ives gold camp, Western Australia: vectors to high-grade ore bodies in Archaean gold deposits? Mineral. Deposita 43, 363–371.
Oppenheimer, C., Moretti, R., Kyle, P.R., Eschenbacher, Al, Lowenstern, J.B., Hervig, R.L., Dunbar, N.W., 2011. Mantle to surface degassing of alkalic magmas at Erebus volcano, Antarctica. Earth Planet. Sci. Lett. 306, 261–271.
Otofuji, Y.I., Tung, V.D., Fujihara, M., Tanaka, M., Yokoyama, M., Kitada, K., Zaman, H., 2011. Tectonic deformation of the southeastern tip of the Indochina Peninsula during its southward displacement in the Cenozoic time. Gondwana Res. 22, 615–627.
Palin, J.M., Xu, Y., 2000. Gilt by association? Origins of pyritic gold ores in the Victory mesothermal gold deposit, Western Australia. Econ. Geol. 95, 1627–1634.
Rudnick, R.L., Gao, S., 2003. Composition of the continental crust. In: Rudnick, R.L. (Ed.), Treatise on GeochemistryThe Crust. vol. 3. Elsevier, pp. 1–64.
Salters, V., Stracke, A., 2004. Composition of the depleted mantle. Geochem. Geophys. Geosyst. 5. http://dx.doi.org/10.1029/2003GC000597.
Sassier, C., Leloup, P.H., Rubatto, D., Galland, O., Yue, Y., Lin, D., 2009. Direct measurement of strain rates in ductile shear zones: a new method based on syntectonic dikes. J. Geophys. Res. 114, B01406. http://dx.doi.org/10.1029/2008JB005597.
Schärer, U., Zhang, L.S., Tapponnier, P., 1994. Duration of strike-slip movements in large shear zones: the Red River belt, China. Earth Planet. Sci. Lett. 126, 379–397.
Searle, M.P., Yeh, M.W., Lin, T.H., Chung, S.L., 2010. Structural constraints on the timing of left-lateral shear along the Red River shear zone in the Ailao Shan and Diancang Shan Ranges, Yunnan, SW China. Geosphere 6, 316–318.
Sheppard, S.M.F., 1986. Characterization and isotopic variations in natural waters. Rev. Mineral. 16, 165–183.
Socquet, A., Pubellier, M., 2005. Cenozoic deformation in western Yunnan (China–Myanmar border). J. Asian Earth Sci. 24, 495–515.
Spurlin, M.S., Yin, A., Horton, B.K., Zhou, J.Y., Wang, J.H., 2005. Structural evolution of the Yushu–Nangqian region and its relationship to syncollisional igneous activity, east-central Tibet. Geol. Soc. Am. 117, 1293–1317.
Sun, X.M., Zhang, Y., Xiong, D.X., Sun, W.D., Shi, G.Y., Zhai, W., Wang, S.W., 2009. Crust and mantle contributions to gold-forming process at the Daping deposit, Ailaoshan gold belt, Yunnan, China. Ore Geol. Rev. 36, 235–249.
Tang, J.X., Wang, C.H., Qu, W.J., Du, A.D., Ying, L.J., Gao, Y.M., 2009. Re–Os isotopic dating of molybdenite from the Yulong porphyry copper–molybdenum deposit in Tibet and its metallogenic significance. Rock Mineral Anal. 28, 215–218 (in Chinese with English abstract).
Tang, Y., Liu, J.L., Tran, M.D., Song, Z.J., Wu, W.B., Zhang, Z.C., Zhao, Z.D., Chen, W., 2013. Timing of left-lateral shearing along the Ailao Shan–Red River shear zone: constraints from zircon U–Pb ages from granitic rocks in the shear zone along the Ailao Shan Range, Western Yunnan, China. Int. J. Earth Sci. 102, 605–626.
Taylor, S.R., Mclennan, S.M., 1985. The Continent Crust: Its Composition and Evolution. Blackwell, London, pp. 57–72.
Wang, P.L., Lo, C.H., Chung, S.L., Lee, T.Y., Lan, C.Y., Thang, T.V., 2000. Onset timing of left-lateral movement along the Ailao Shan–Red River shear zone: ^{40}Ar–^{39}Ar dating

constraint from the Nam Dinh Area, northeastern Vietnam. J. Asian Earth Sci. 18, 281–292.
Wang, J.H., Yin, A., Harrison, T.M., Grove, M., Zhang, Y.Q., Xie, G.H., 2001a. A tectonic model for Cenozoic igneous activities in the eastern Indo-Asian collision zone. Earth Planet. Sci. Lett. 188, 123–133.
Wang, J.H., Qi, L., Yin, A., Xie, G.H., 2001b. Emplacement age and PGE geochemistry of lamprophyres in the Laowangzhai gold deposit, Yunnan, SW China. Sci. China Ser. D Earth Sci. 44 (Suppl.), 146–154.
Wang, J.H., Yin, A., Harrison, T.M., Grove, M., Zhou, J.Y., Zhang, Y.Q., Xie, G.H., 2003. Thermochronological constraints on two pulses of Cenozoic high-K magmatism in eastern Tibet. Sci. China Ser. D Earth Sci. 46, 719–729.
Wang, D.H., Chen, Y.C., Xu, J., Yang, J.M., Xue, C.J., Yan, S.H., 2005. Cenozoic Mineralization in China. Geological Publishing House, Beijing, pp. 1–853.
Wang, C.H., Tang, J.X., Chen, J.P., Hao, J.H., Gao, Y.M., Liu, Y.W., Fan, T., Zhang, Q.Z., Ying, L.J., Chen, Z.J., 2009. Chronological research of Yulong copper–molybdenum porphyry deposit. Acta Geol. Sin. 83, 1445–1455 (in Chinese with English abstract).
Wang, Q.F., Deng, J., Li, C.S., Li, G.J., Yu, L., Qiao, L., 2014. The boundary between the Simao and Yangtze blocks and their locations in Gondwana and Rodinia: constraints from detrital and inherited zircons. Gondwana Res. 26, 438–448.
Xiong, D.X., Sun, X.M., Shi, G.Y., 2007. Geochemistry and Metallogenic Model of Ailaoshan Cenozoic Organic Gold Belt in Yunnan Province. China. Geological Publishing House, Beijing, pp. 80–98 (in Chinese with English abstract).
Xu, Z.Q., Li, H.B., Tang, Z.M., Qi, X.X., Li, H.Q., Cai, Z.H., 2011. The transformation of the terrain structures of the Tibet plateau through large-scale strike-slip faults. Acta Petrol. Sin. 27, 3157–3170 (in Chinese with English abstract).
Yang, L.Q., Deng, J., Zhao, K., Liu, J.T., 2011. Tectono-thermochronology and gold mineralization events of orogenic gold deposits in Ailaoshan orogenic belt, Southwest China: geochronological constraints. Acta Petrol. Sin. 27, 2519–2532 (in Chinese with English abstract).
Yin, A., Harrison, T.M., 2000. Geologic evolution of the Himalayan–Tibetan orogen. Annu. Rev. Earth Planet. Sci. 28, 211–280.
Zaw, K., Meffre, S., Lai, C.K., Burrett, C., Santosh, M., Graham, I., Manaka, T., Salam, A., Kamvong, T., Cromie, P., 2014. Tectonics and metallogeny of mainland Southeast Asia — a review and contribution. Gondwana Res. 26, 5–30.
Zhang, L.S., Schärer, U., 1999. Age and origin of magmatism along the Cenozoic Red River shear belt, China. Contrib. Mineral. Petrol. 134, 67–85.
Zhang, J.J., Zhong, D.L., Sang, H.Q., Zhou, Y., 2006. Structural and geochronological evidence for multiple episodes of tertiary deformation along the Ailaoshan–Red River shear zone, southeastern Asia, since the Paleocene. Acta Geol. Sin. Engl. ed. 80, 79–96.
Zhang, J., Deng, J., Li, S.H., Yan, N., Yang, L.Q., Ma, N., Wang, Q.F., Gong, Q.J., 2010. Petrological characteristics of magmatites and their relationship with gold mineralization in the Chang'an gold deposit in southern Ailaoshan metallogenic belt. Acta Petrol. Sin. 26, 1740–1750 (in Chinese with English abstract).
Zhao, X., Yu, X.H., Mo, X.X., Zhang, J., Lu, B.X., 2004. Petrological and geochemical characteristics of Cenozoic alkali-rich porphyries and xenoliths hosted in western Yunnan province. Geoscience 18, 217–228 (in Chinese with English abstract).
Zhao, Y., Wang, Q.F., Sun, X., Li, G.J., 2013a. Characteristics of ore-forming fluid in the Zhenyuan gold orefield, Yunnan Province, China. J. Earth Sci. 24, 203–211.
Zhao, K., Yang, L.Q., Li, P., Xiong, Y.Q., 2013b. Morphology and chemistry composition of pyrite in the Laowangzhai gold deposit, Ailaoshan orogenic belt, SW China. Acta Petrol. Sin. 29, 3937–3948 (in Chinese with English abstract).
Zhong, D.L., 1998. The Paleo-Tethyan Orogenic Belts, Western Yunnan and Sichuan Provinces. Science Press, Beijing, pp. 1–231 (in Chinese).
Zhu, X.P., Mo, X.X., White, N.C., Zhang, B., Sun, M.X., Wang, S.X., Zhao, S.L., Yang, Y., 2009. Geology and metallogenetic setting of the Habo porphyry Cu (Mo–Au) deposit, Yunnan. Acta Petrol. Sin. 83, 1915–1928 (in Chinese with English abstract).
Zi, J.W., Cawood, P.A., Fan, W.M., Wang, Y.J., Tohver, E., 2012. Contrasting rift and subduction-related plagiogranites in the Jinshajiang ophiolitic mélange, southwest China, and implications for the Paleo-Tethys. Tectonics http://dx.doi.org/10.1029/2011TC002937.
Zindler, A., Hart, S.R., 1986. Chem. geodyn. Ann. Rev. Earth Planet. Sci. 14, 493–571.